

Communication

A Novel Passive Implantable Differential Mechanism to Restore Individuated Finger Flexion during Grasping following Tendon Transfer Surgery: A Pilot Study

Suraj Chakravarthi Raja ¹, Won Suk You ², Kian Jalaleddini ³, Justin C. Casebier ⁴,
Nina R. Lightdale-Miric ⁵, Vincent R. Hentz ⁶, Francisco J. Valero-Cuevas ^{1,7,†}
and Ravi Balasubramanian ^{4,*†}

¹ Ming Hsieh Department of Electrical and Computer Engineering, University of Southern California, Los Angeles, CA 90007, USA

² AstroForge, Inc., 15261 Connector Ln, Huntington Beach, CA 92649, USA

³ iKinesia Inc., 490 Boul Provencher, Brossard, QC J4W 1Y4, Canada

⁴ Collaborative Robotics and Intelligent Systems (CoRIS) Institute, School of Mechanical, Industrial and Manufacturing Engineering (MIME), Oregon State University, Graf Hall 315, Corvallis, OR 97331, USA

⁵ Children's Hospital, Los Angeles, CA 90027, USA

⁶ The Chase Center for Hand and Upper Limb Surgery, Stanford University, Stanford, CA 94305, USA

⁷ Alfred E. Mann Department of Biomedical Engineering, University of Southern California, Los Angeles, CA 90007, USA

* Correspondence: ravi.balasubramanian@oregonstate.edu

† Joint senior authors.



Citation: Chakravarthi Raja, S.; You, W.S.; Jalaleddini, K.; Casebier, J.C.; Lightdale-Miric, N.R.; Hentz, V.R.; Valero-Cuevas, F.J.; Balasubramanian, R. A Novel Passive Implantable Differential Mechanism to Restore Individuated Finger Flexion during Grasping following Tendon Transfer Surgery: A Pilot Study. *Appl. Sci.* **2023**, *13*, 5804. <https://doi.org/10.3390/app13095804>

Academic Editors: Verónica Gracia-Ibáñez, Néstor José Jarque-Bou and Margarita Vergara

Received: 13 January 2023

Revised: 29 April 2023

Accepted: 2 May 2023

Published: 8 May 2023



Copyright: © 2023 by the authors. Licensee MDPI, Basel, Switzerland. This article is an open access article distributed under the terms and conditions of the Creative Commons Attribution (CC BY) license (<https://creativecommons.org/licenses/by/4.0/>).

Abstract: Tendon transfer surgery is often used to restore hand grasp function following high median-ulnar nerve palsy. This surgery typically reroutes and sutures the tendon of the extensor carpi radialis longus (ECRL) muscle to all four flexor digitorum profundus (FDP) tendons of the hand, coupling them together. This makes it difficult to grasp irregularly shaped objects. We propose inserting a novel implantable passive device between the FDP tendons to surgically construct a differential mechanism, enabling the fingers to individually adapt to the irregular contours during grasping. These passive implants with no moving parts are fabricated from biocompatible materials. We tested the implants' ability to create differential flexion between the index and middle fingers when actuated by a single muscle in two human cadaver hands using a computerized closed-loop control paradigm. In these cadaveric models, the implants enabled significantly more differential flexion between the index and middle fingers for a wide range of donor tendon tensions. The implants also redistributed fingertip forces between fingers. When grasping uneven objects, the difference in contact forces between fingers reduced by nearly 23% compared to the current suture-based surgery. These results suggest that self-adaptive grasp is possible in tendon transfers that drive multiple distal flexor tendons.

Keywords: implant design; median-ulnar nerve injury; finger flexion; tendon transfer; hand surgery; grasp

1. Introduction

The high median-ulnar nerve injury paralyzes the *flexor digitorum profundus* (FDP) muscle partially and the *flexor digitorum superficialis* (FDS) muscle completely, resulting in a limited grasping function. One current surgical solution to restore flexion of the four fingers is a tendon transfer surgery where the four FDP tendons of insertion are rerouted and sutured to the single tendon of insertion of the donor *extensor carpi radialis longus* (ECRL) muscle, a wrist extensor innervated by another nerve, namely, the radial nerve [1–5]. However, this procedure has a fundamental drawback: it couples the excursion of the previously independent FDP tendons to the single ECRL tendon. This locks the

movement of all four fingers even if just one finger is unable to move after making contact with an object during grasping; therefore, not all fingers are able to make contact when grasping irregularly-shaped objects, and even simple tasks, such as holding an apple, become challenging [6].

Prior work has documented the disappointing grasping function that arises from coupled finger movement when multiple tendons are sutured to one muscle [7,8]. Specifically, the coupled finger movement leads to (i) incomplete, weak, and unbalanced grasps [7]; (ii) greater muscle force required to create full multi-finger contact, because the tendons of the open fingers need to be stretched to close them once one finger makes contact; and (iii) uneven tendon tensioning. Additionally, challenges arise from anatomical differences between patients and a limited set of donor muscles. For example, even when the number of functioning muscles is highly limited, the standard of care will not assign more than one function (such as finger and thumb flexion) to the donor muscle due to the suture's coupling effect [7]. Unfortunately, the hand grip remains weak post-surgery, because the suture couples the fingers and the fingers do not adapt to an object's shape. This greatly reduces the patient's independence and ability to work.

To improve post-operative quality of life, we have developed a passive device implantable between the FDP tendons and the donor ECRL muscle to construct a network of *differential mechanisms*. This network of differential mechanisms will enable the fingers to continue to flex even if the other finger or fingers is/are locked after having already made contact. These devices have been patented by Dr. Valero-Cuevas and Dr. Balasubramanian along with Dr. Homayouni (per U.S. Patents 9,925,035 and 10,595,984 [9,10]). Our previous simulation and human cadaver studies showed that such a network of implants embodied as hierarchically-arranged pulleys improved grasping of irregular objects [11]. However, the pulleys are too bulky and a low-profile embodiment is desired to create similar differential action.

In this work, we explore the efficacy of two low-profile implant embodiments (a rod embodiment and a U-shaped embodiment; see Figure 1, panels A1 and B1, respectively), with the goal of advancing these implants toward clinical adoption. These implants form a triangle with the bifurcation point of the FDP tendons from the ECRL acting as the triangle apex [6]. In terms of mechanical action, this triangle would translate as the muscle contracts. However, the triangle also introduces a rotational degree-of-freedom about the triangle apex. This enables passive differential action between the index and middle finger, even if they are driven by one muscle. The embodiment's efficacy will be measured in terms of the improved evenness/balance in the force distribution between the two fingers and compared with the force distribution seen in the current suture-based surgery.

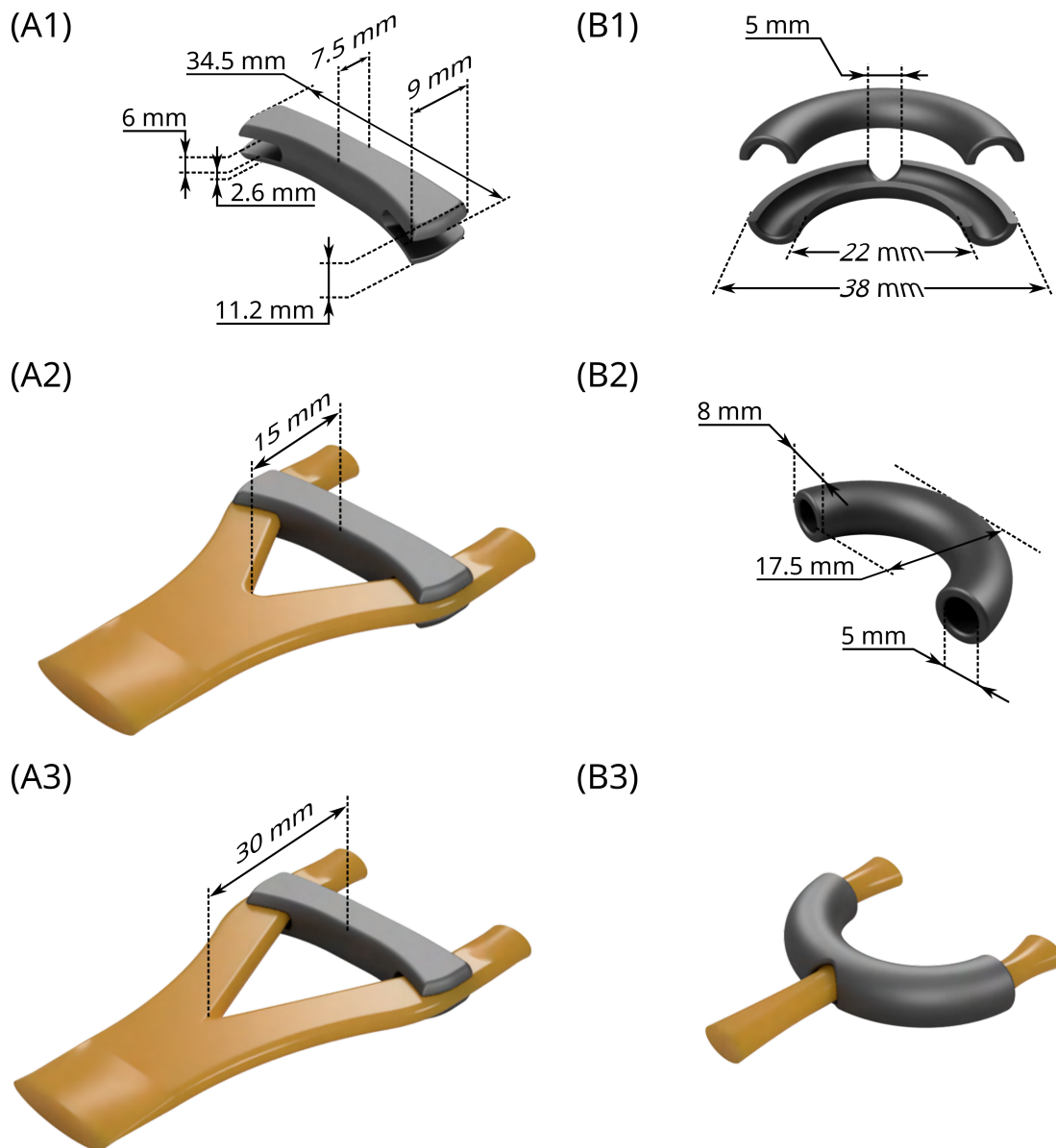


Figure 1. CAD models of two low-profile implants (rendered in gray). Panel (A1) depicts the *rod implant*. This implant may be positioned close to (see panel (A2)) or further away (see panel (A3)) from the bifurcation of the tendon (rendered in gold). However, the *U implant* (panels (B1), (B2)) is a two-piece implant which fixes (as seen in panel (B3)) around the bifurcating tendon. Therefore, its position cannot be changed.

2. Materials and Methods

This study tested whether our implants improved the ability of the index and middle fingers to perform differential flexion when driven by a tendon transfer, as more equal force distributions across fingers are desired when grasping irregular objects. Differential flexion is the individuated force application by one finger (say, the middle finger) when the other (say, the index finger) is constrained by external contact, even if both fingers are driven by one flexor muscle, as seen in Figure 2.

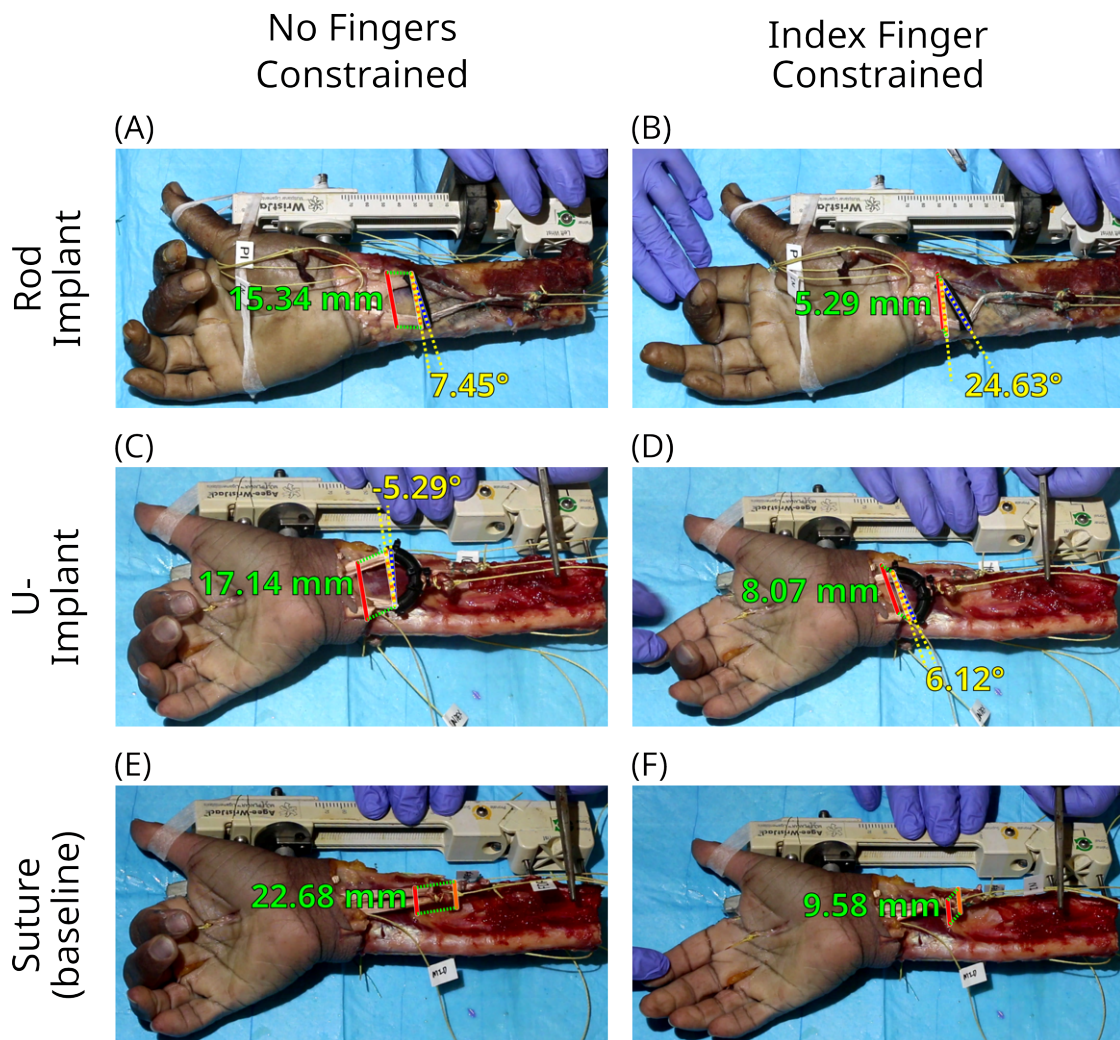


Figure 2. Fixing and testing the implants: The panels depict fully prepared cadaver hands both with and without one of the two implant types evaluated in this study. The first column of panels features index and middle finger flexion when neither finger is constrained. The second column of panels features middle finger flexion when the index finger is constrained. Panels (A,B) feature a cadaver specimen with a *rod implant* attached distal to the bifurcation point of FDP tendons. Panels (C,D) showcase the same but with a *U-implant* attached around the bifurcation point. Panels (E,F) display the outcome of the *baseline suture-based* surgery. In panels (A,C) the implants translated proximally to allow both fingers to flex. Upon constraining the index finger (B,D), the implants sacrificed this ability to translate proximally. To accommodate the movement of the unconstrained middle finger, they instead rotated further counterclockwise as more tension is applied by the donor tendon. However, the suture-based baseline case could only translate (see panel (E)). So, when the index finger was constrained, the middle finger barely moved (see panel (F)).

2.1. Cadaver Preparation with Implants

We tested two 3D-printed rigid polyurethane (RPU) [12] implants. In Figure 1, the rod implant in panel A1 could form shorter (15 mm; see panel A2) or taller (30 mm; see panel A3) triangles. The triangle height of the U implant was fixed by the geometry of the implant as seen in Figure 1 (panels B1–B3).

We used two fresh-frozen cadaveric arms disarticulated at the elbow. Both suture- and implant-based procedures were tested on each arm. Hand surgeons tagged the insertion tendons of the FDP and ECRL, and resected muscle tissue. The wrist joint was stabilized and fixed by an Agee-WristJack® [13,14], as seen in Figure 2. We sutured inelastic Kevlar® cables (McMaster-Carr part #8800K43, 0.038" diameter high-strength high-temperature para-aramid thread [15]) to the FDP, *extensor indicis proprius* (EIP), and *extensor digitorum communis* (EDC) tendons of the index and middle fingers. Both FDP tendons were coupled to and driven by a single DC motor simulating the ECRL muscle. To one specimen, we attached a rod implant distal to the FDP tendon bifurcation point (Figure 2, panels A,B). To the other, we attached a U implant (Figure 2, panels C,D). After conducting the study to evaluate the differential flexion of each hand specimen, the implants were removed (as seen in Figure 2, panels E,F) to repeat the study for the current state-of-the-art suture-based procedure.

2.2. Actuation and Sensing

The proximal end of the ECRL tendon's Kevlar cable was attached to a DC motor through a cable tension sensor for active control (Figure 3, labels A,D). Using an experimental test platform similar to our previous work [16,17], the ECRL tendon tension was set by a proportional-integral force controller via a National Instruments™ (NI) data acquisition system. Similar actuation of the EIP and EDC tendons allowed us to extend and reset the fingers to the starting point between finger flexion trials. Additionally, the hand was held with a "victory-V" gesture at all times by passively tensioning the index finger's *dorsal interosseous* and the middle finger's *palmar interosseous* while folding the other digits, as illustrated in Figure 3. We understand that this gesture is not a typical hand posture used in functional activities. Additionally, grasping requires flexion at the interphalangeal joints, which are splinted in this work. However, to show proof-of-concept of the mechanical efficacy of the implants to distribute force between two output tendons driven by a single muscle, the "victory-V" based on flexion only at the metacarpal joints is sufficient. If the distal joints were indeed free to move, the differential action enabled by the implant at the metacarpal joints would have been available to the distal joints as well. The "victory-V" gesture also ensured that the two fingers being tested do not interfere with one another.

We attached a custom instrumented paddle with two hemicylindrical contact- and force-sensing finger pads to the wrist joint of an Omron® AdeptSix 300 industrial robot [18] (see Figure 3B,C). This robot enabled positioning and orienting the paddle so the paddle's rotational axis was centered between the two fingers. Additionally, the plane of the paddle's instrumentation was parallel to the two fingers such that both fingers (when at rest) were barely making contact with the paddle. Rotating the robot's wrist allowed us to change the paddle orientation per our experimental protocol.

2.3. Testing Protocol

We simulated finger contact with the contours of irregular objects by gradually rotating and holding the instrumented paddle at multiple orientations from $\pm 3^\circ$ to $\pm 30^\circ$ at 3° intervals. A baseline tendon tension of 1 newton (N) simulated muscle tone on the ECRL, EIP, and EDC tendons to prevent tendon slack. We then measured the force applied by each finger on its paddle force plate for different simulated FDP tendon tensions from 3 N to 30 N.

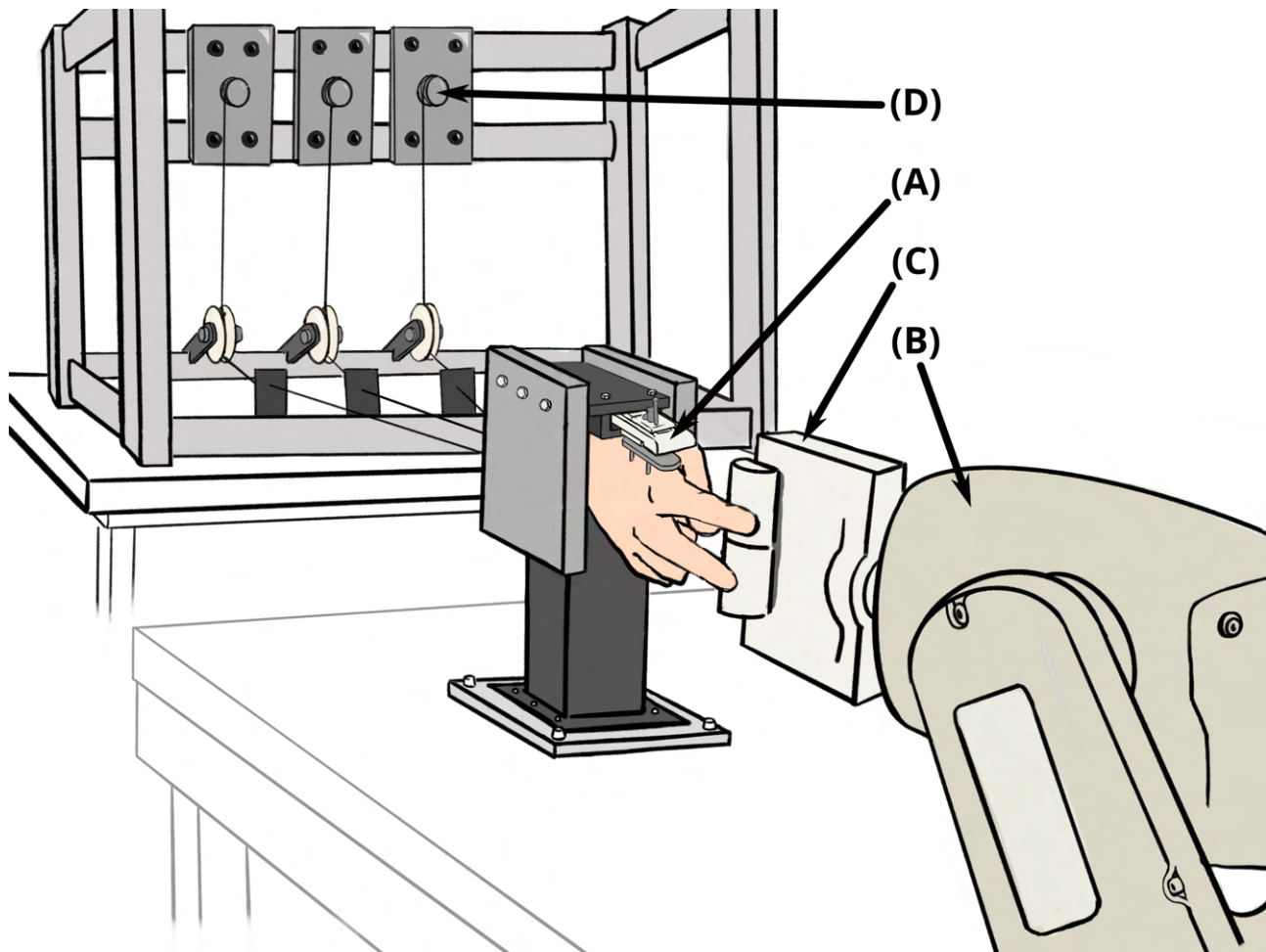
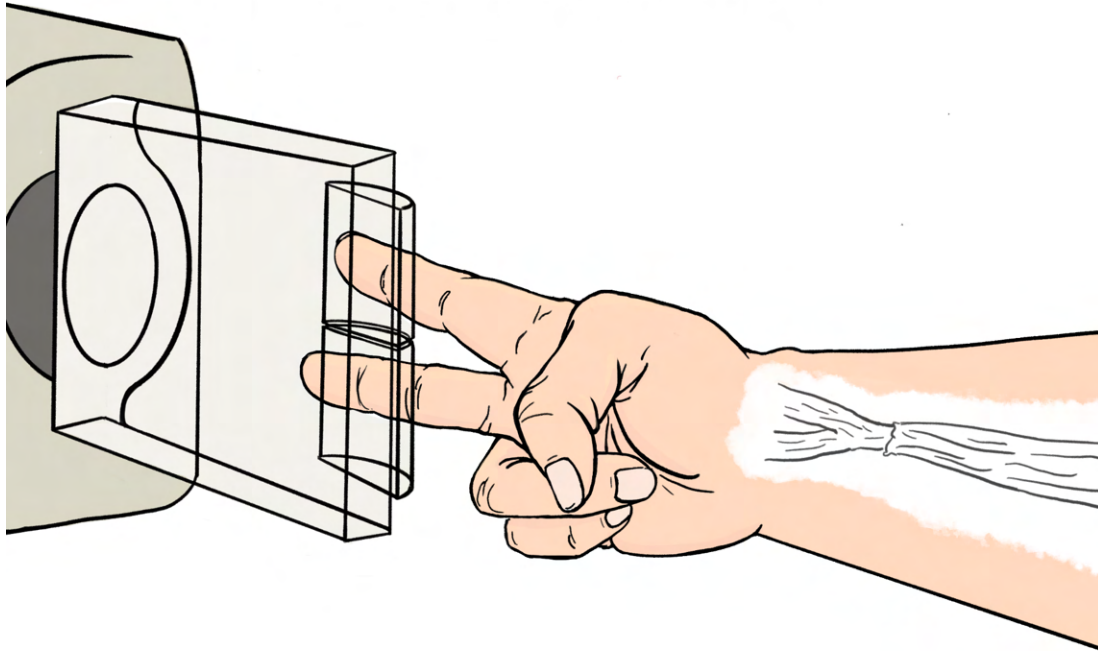


Figure 3. Experimental Setup: The cadaver hand specimen is mounted to an Agee-WristJack® (A) using bone pins drilled into the radial and ulnar bones to stabilize the wrist joint. The specimen is also attached to the experiment platform using the WristJack. A robotic arm (B) positions a sensorized paddle (C) so each finger can individually push on a force plate. The robotic arm can also rotate the paddle to simulate the contours of irregular objects. The donor ECRL flexor tendon, and the extensor EIP and EDC tendons are actuated by force-controlling DC motors (D). Illustrated by Sabrina Teo.

Both cadavers underwent the first of three test scenarios: implant (either rod or U implant)—this evaluated the implants' and suture performances gliding freely (see Figure 4, panel B). Since the rod implant could be repositioned, it was tested using this scenario for two positions (15 mm, 30 mm distal) from the tendon bifurcation point. The next scenario simulated scarring-related tissue adhesion of the implants using 3M™ Vetbond™. Finally, we removed the implants to test the suture-based surgery (see Figure 4, panel A).

We compared the efficacy of each implant-/suture-based surgery in maintaining equal index and middle fingertip forces as paddle orientation and input tendon tension changed. The *difference in fingertip forces* quantifies the absolute deviation from the ideal zero difference in forces (see Figure 5, panel D: green dashed line). Similarly, we also quantified the *variation in fingertip force difference due to input tendon tension* at each paddle rotation angle as the absolute deviation of its fingertip force difference from the mean fingertip force difference (see Figure 5, panel D: lilac dashed line) averaged across all tendon tensions.

(A) Suture-based approach



(B) Implant-based approach

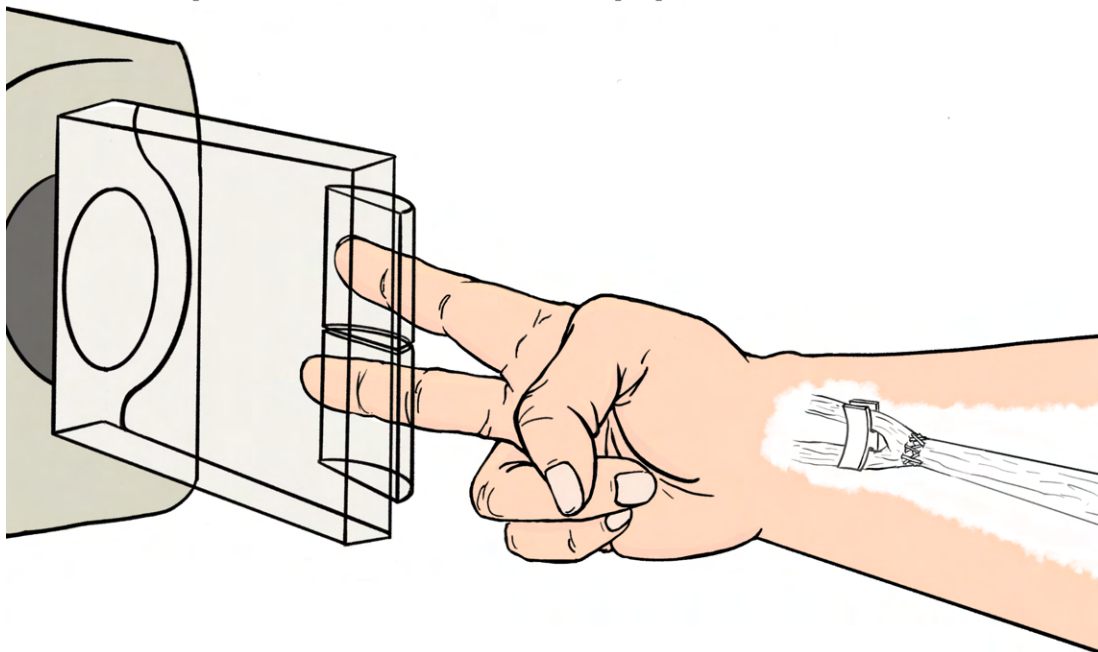


Figure 4. Testing protocol: It involves rotating a properly positioned instrumented paddle to simulate the index and middle fingers attempting to adapt to the contours of irregular objects. We test both the current state-of-the-art suture-based surgical technique (panel (A); as a baseline) and our proposed implant-based technique (panel (B); with two types of implants). Illustrated by Sabrina Teo.

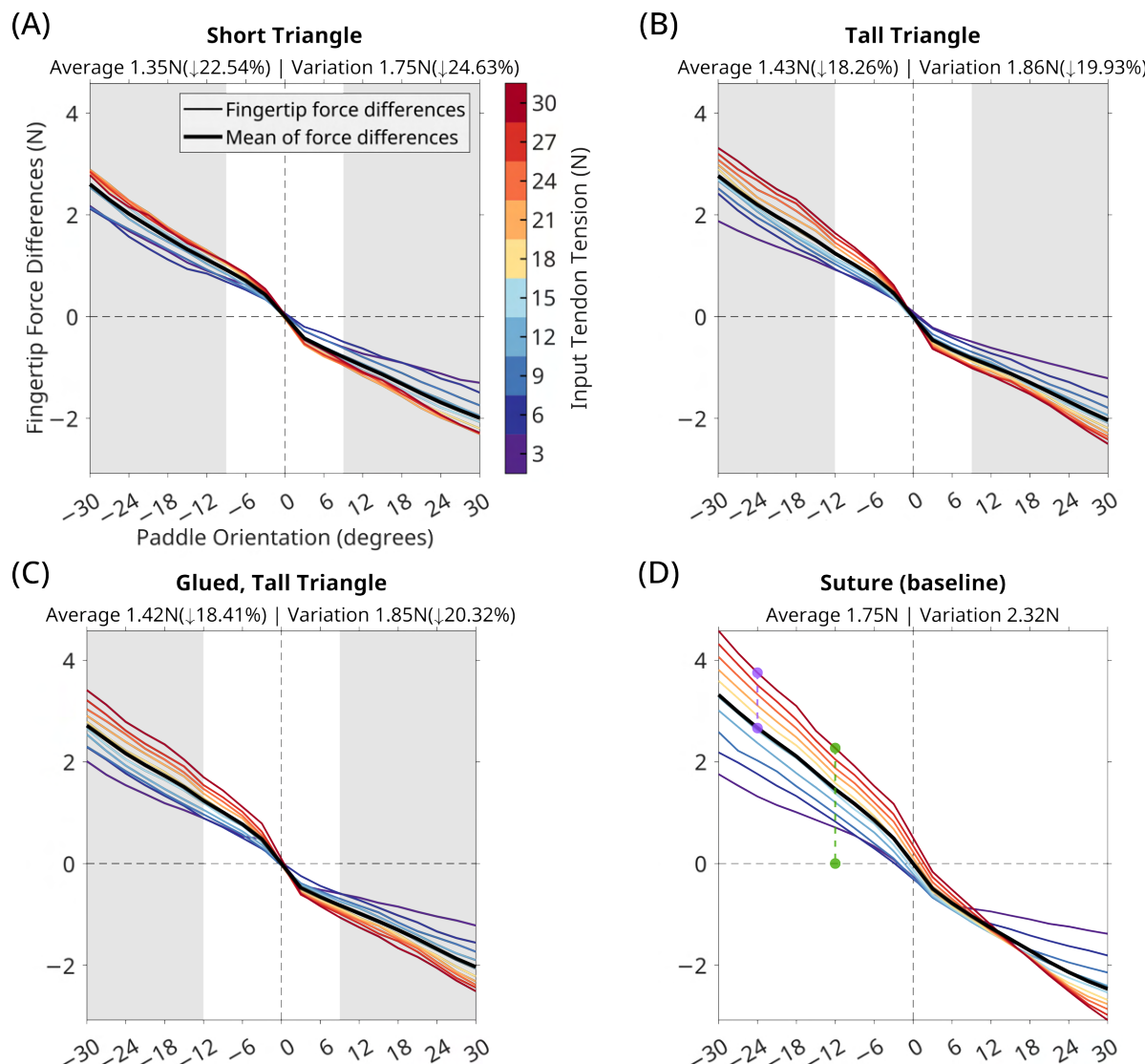


Figure 5. Difference between index and middle fingertip forces measured at various paddle orientations and tendon tensions with and without the rod implant: (A) short triangle configuration; (B) tall triangle configuration; (C) glued tall triangle configuration; and (D) baseline suture configuration. The gray background highlights paddle orientations for which fingertip force differences were significantly different compared to the baseline suture configuration. The green dashed line in panel (D) highlights the fingertip force difference of the suture case for 30 N tendon tension at -12° paddle orientation. Similarly, the lilac dashed line highlights the force difference variation at -24° paddle orientation. Equations (1) and (2) are computed using fingertip forces measured at every orientation and input tension.

Mean Average Error (MAE) for each of these two quantities—computed as the average of all deviations across every paddle rotation angle for each input tendon tension—gives us two metrics (see Equations (1) and (2)) for each of the following test configurations:

- Rod implant (short tendon triangle)—free moving.
- Rod implant (tall tendon triangle)
 - Free moving
 - Glued to surrounding tissue to simulate postoperative scarring.

- U implant
 - Free moving
 - Glued to surrounding tissue to simulate postoperative scarring.
- Baseline suture approach—free moving.

$$MAE_{fingertip\ force\ differences} = \frac{1}{m \cdot n} \left[\sum_{i}^{'m'} \text{tendon tensions} \sum_{j}^{'n'} \text{rotation angles} |fingertip\ force\ difference_{i,j}| \right] \quad (1)$$

$$MAE_{force\ difference\ variation} = \frac{1}{m \cdot n} \left[\sum_{i}^{'m'} \text{tendon tensions} \sum_{j}^{'n'} \text{rotation angles} |force\ difference_{i,j} - \text{mean force difference}_i| \right] \quad (2)$$

3. Results

3.1. Rod Implant

Our comparisons are enabled by evaluating the difference in fingertip forces between the index and middle fingers for each of the three test configurations of the rod implant (Figure 5, panels A–C) as well as the suture-based procedure (panel D), across every paddle orientation and donor tendon tension. We then computed the MAEs as comparison metrics for each configuration using Equations (1) and (2). The short-triangle rod implant (panel A) was the best performer with an average fingertip force difference of 1.35 N—a 22.57% reduction in fingertip force differences relative to the suture-based baseline configuration (seen in panel D) across all paddle orientations and tendon tensions. This configuration also had the lowest variation in these fingertip force differences due to tendon tension at 1.75 N—a 24.66% reduction compared to the suture-based procedure. This reduction could mean the difference in the ability of the hand to acquire an irregularly-shaped object without twisting it as it is grasped. With a *p*-value < 0.05%, this configuration also showcased significantly different fingertip force differences for paddle orientations in the range [−30°, −9°] and [9°, 30°] compared to the baseline. These results show promise for clinical impact [19,20].

While the tall triangle configurations—both free-moving (panel B) and glued (panel C)—do not perform as well, they did outperform the baseline with average reductions in fingertip force differences of over 18% (compared to the baseline). These cases also displayed similar reductions in the variation of fingertip force differences due to tendon tension of about 20%. This suggests that a larger triangle formed by the rod implant with the bifurcating tendons has lower force redistribution capabilities. Additionally, the tissue adhesion simulated by gluing the implant did not significantly alter performance. The exact values are listed in Table 1.

These differences in fingertip forces were computed from the fingertip forces of the index and middle fingers for each test configuration of the rod implant-based and suture-based procedures (see Figure 6, panels A–D). The negative orientations pushed against and caused extension of the index finger. Positive orientations did the same for the middle finger. The figure clearly shows that these extensions caused the fingertip force to increase. This is because neither the implant nor the suture can perfectly redistribute forces. Unsurprisingly, increasing tendon tension proportionately increased fingertip forces.

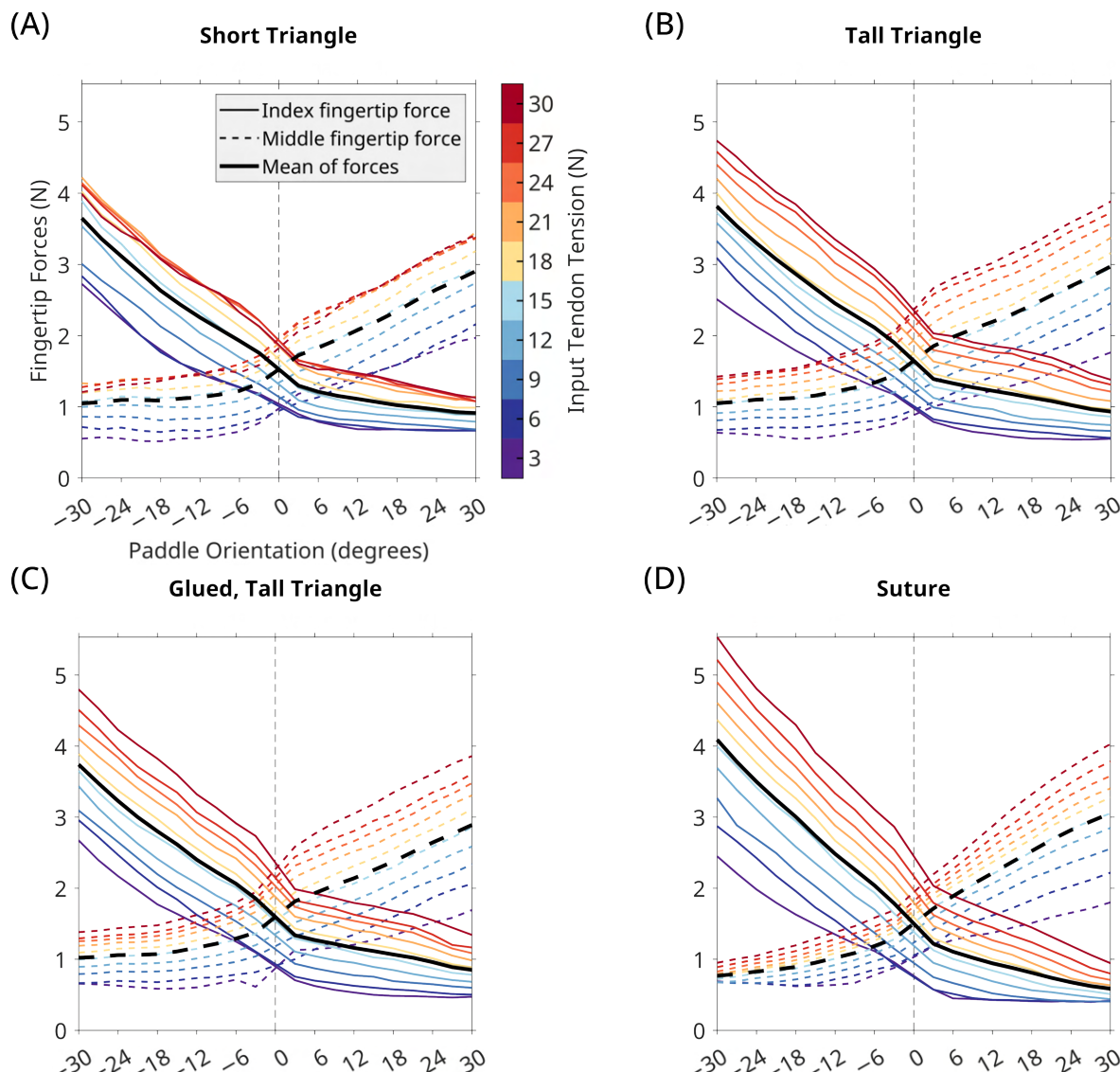


Figure 6. Index and middle fingertip forces measured at various paddle orientations and tendon tensions with and without the rod implant: (A) short triangle configuration; (B) tall triangle configuration; (C) glued tall triangle configuration; and (D) baseline suture configuration. The negative paddle orientations force the index finger to extend and increase its fingertip force. Positive orientations do the same for the middle finger.

Here too, we see that the free-moving short triangle configuration had the best performance, showcasing the lowest variations/spread of absolute fingertip forces relative to tendon tension. Both the free-moving and glued tall triangle configurations performed about the same as each other and not, as well as the first case but also outperformed the suture configuration. However, for a given tendon tension, maximum fingertip forces were lower with the implant since it redistributed forces between the two fingers.

Table 1. A performance comparison of all test configurations relative to the suture-based procedure—computed from the data in Figures 5 and 7 using Equations (1) and (2).

Configuration	Average Difference in Fingertip Forces (Lower MAE Is Better)	Variation in Fingertip Force Differences Due to Input Tendon Tension (Lower MAE Is Better)	Paddle Orientations for Which Implant Outperforms Baseline (<i>p</i> -Value < 0.05%)
Rod implant			
short triangle	↓ 22.54% (1.35N MAE)	↓ 24.63% (1.75N MAE)	[−30°, −9°] and [9°, 30°]
tall triangle	↓ 18.26% (1.43N MAE)	↓ 19.93% (1.86N MAE)	[−30°, −12°] and [9°, 30°]
glued tall triangle	↓ 18.41% (1.42N MAE)	↓ 20.32% (1.85N MAE)	[−30°, −12°] and [9°, 30°]
baseline suture	_____ (1.75N MAE)	_____ (2.32N MAE)	_____
U implant			
U implant	↓ 19.54% (1.28N MAE)	↓ 11.85% (1.86N MAE)	[−30°, −18°] and [27°, 30°]
glued U implant	↓ 7.66% (1.46N MAE)	↓ 11.86% (1.86N MAE)	_____
baseline suture	_____ (1.59N MAE)	_____ (2.11N MAE)	_____

3.2. U Implant

Figure 7 plots the difference in fingertip forces for two test configurations (free implant (panel A), glued implant (panel B)) of the U implant along with the suture-based procedure (panel C). The U implant also redistributed forces resulting in lower fingertip forces relative to the baseline. From panels (A) and (B), the U implant did reduce the difference in fingertip forces. However, this is where the U implant’s results diverge from the rod implant. The average difference in fingertip forces (computed using Equation (1)) shows that both the free-moving and glued U implant configurations perform worse than short-triangle configuration and about on par with the tall-triangle configuration of the rod implant (see Table 1). Their variation due to tendon tension (computed using Equation (2)) is even worse, performing lower than even the least performing tall-triangle rod implant configuration. In the case of the U implant (panel A), there were a few outliers in fingertip forces that occurred potentially due to controller glitches or spurious stiction in the robotic testbed. These six outliers (out of 200 trials) were omitted for this case when computing the mean fingertip forces but are marked in the figure in the interest of transparency. Finally, we only saw significant differences between the free U implant and the baseline for a small paddle orientation region ([−30°, −18°] and [27°, 30°]). These results do not suggest as much promise of clinical translation for the U implant as the rod implant.

Figure 8 depicts the fingertip forces of the index and middle fingers for the three applicable test configurations. Much like with the rod implant, the redistribution is less than perfect, with extensions resulting in larger fingertip forces. Also, increasing tendon tensions generally did increase fingertip forces. The six outliers trials that were omitted when computing the mean fingertip forces are marked in this figure as well.

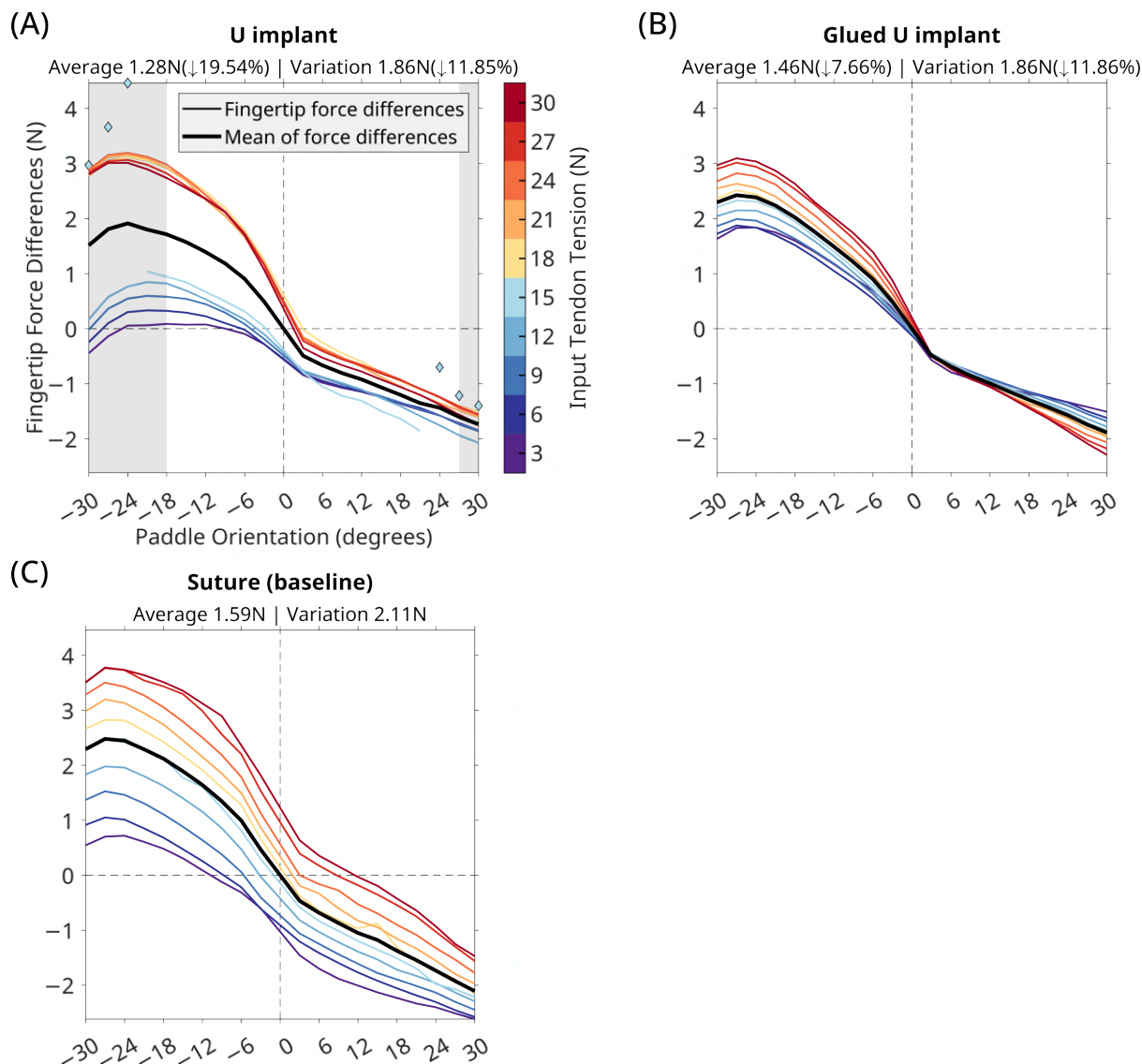


Figure 7. Difference between index and middle fingertip forces measured at various paddle orientations and tendon tensions with and without the *U implant*: (A) *U implant* configuration; (B) glued *U implant* configuration; and (C) baseline suture configuration. The gray background highlights paddle orientations for which fingertip force differences were significantly different compared to the baseline suture configuration. The diamond markers in panel (A) represent outliers that have been omitted when computing mean fingertip forces.

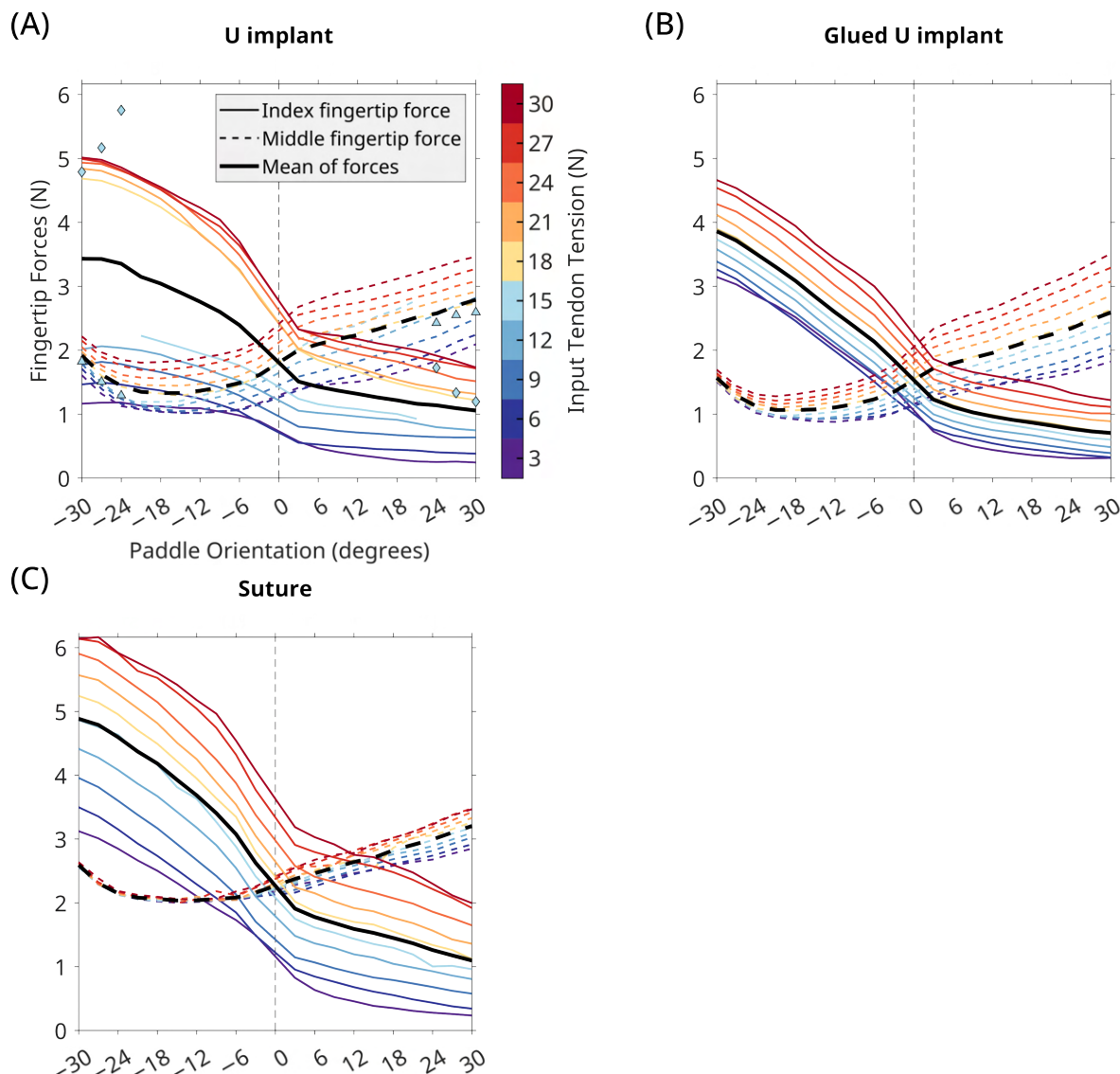


Figure 8. Index and middle fingertip forces measured at various paddle orientations and tendon tensions with, and without the U implant: (A) U implant configuration; (B) glued U implant configuration; and (C) baseline suture configuration. The negative paddle orientations force the index finger to extend and increase its fingertip force. Positive orientations do the same for the middle finger. The diamond markers in panel (A) represent outliers in index fingertip forces that have been omitted when computing mean fingertip forces. The triangle markers represent the same for middle fingertip forces.

4. Discussion

Tendon transfer surgery has been the preferred approach to restore hand function after high median-nerve palsy since 1974, when coupling the ECRL tendon to the FDP of the index and/or middle fingers was first used to restore grasp and pinch function [5]. With ulnar nerve innervation, the FDP to the ring and small fingers may remain functional. However, pinch and power grip are greatly diminished without the FDS and the flexor pollicis longus (FPL). While the outcomes of these surgeries have demonstrated ability to flex the index and middle finger in a key pinch or coupled grasp using all fingers, individuated finger function was never achieved and leaves the patient without the ability to adjust finger flexion and grasp forces when grasping irregularly-shaped objects.

The results (Section 3) of this cadaveric study demonstrated that our passive implant can restore up to 22.54% of individuated finger flexion and force production in the same

ECRL-to-FDP tendon transfer surgery. There is also up to 24.63% reduction in variation with changes to input tendon tension. This suggests that it could clinically improve grasp performance independent of input tensions [19,20].

4.1. Implant Performance

While each implant was trialled on a different hand specimen, their performances were normalized against the baseline suture-based scenario conducted on the same specimen. This allowed us to comfortably compare their relative performances.

Table 1 shows that the implants evened out finger forces (i.e., reduced average differences across fingertip forces). The rod implant (with >20% MAE reductions) consistently outperformed the U implant (with <20% MAE reductions) for a wide range of paddle orientations ($[-30^\circ, -12^\circ]$ and $[9^\circ, 30^\circ]$). This remains true even in the glued configuration, which simulated tissue adhesion resulting from scarring. Additionally, in Figure 8 panel (A), we see that with the U implant, the index finger did not apply much force at lower tendon tensions. This problem may have arisen due to minor surgical inconsistencies that the U implant was unable to accommodate, as well as the rod implant.

Considering these promising preliminary results, the *rod implant* is the clear candidate for future work and implant development as we move towards testing the biomechanical efficacy of arranging these implants hierarchically to achieve differential action across four fingers in a large-scale human cadaver study, before eventual clinical trials and United States Food and Drug Administration (FDA) approval.

4.2. Surgical Considerations

The passive implants only introduced one additional suturing step, which added, at most, 15 minutes to the surgery. Anatomically, tendon excursion and alignment with the forearm and carpal tunnel are similar to end-to-end or end-to-side tendon transfers [21–25]. Importantly, surgical revision, if required, would simply mean removing the implant.

The implant could also allow customizing the range of motion and force production of the fingers. This could be achieved by changing the implant's geometry to form a non-isosceles triangle with the tendons, or by altering the rest angle of the implant, or even modifying the FDP tendon length attached to the implant. The rod implant also accommodated for small variations and inaccuracies in measuring tendon lengths prior to suturing without loss of function as would be the case in suture-based approaches. This would simplify the surgery and potentially improve outcomes. The rod implant, with its one-piece monolithic design was also easier to install and suture compared to the U implant.

At flexed postures, we recorded the translations of the implants' centers along with their mediolateral shifts (see Table 2). The implants' rotations were also measured. This was repeated with both fingers unconstrained and with only the index finger constrained. Comparing the two cases, the implants' rotation more than compensated their reduced translation (when compared to the baseline suture case) as a result of the constraints on the index finger. This allowed the middle finger to continue flexing (see Figure 2)—as is the purpose of the implant. This was not the case with the current state-of-the-art suture-based approach since it did not have the rotational degree-of-freedom introduced by the implant.

The mediolateral translation of the rod implant ranged from 0.5 mm to 5.08 mm—unequal finger constraints increased it. However, for the U implant, constraining the index finger reduced the mediolateral translation from 7.06 mm to 3.72 mm. It is important to note for surgical technique that mediolateral translations are also influenced by the routing of the donor tendon.

Table 2. Comparing the translations and rotation of the implants (and suture) when constraining only the index finger versus keeping both fingers unconstrained—measurements from one specimen (see Figure 2).

		Rod Implant	U Implant	Baseline Suture
Translation (mm)	Both fingers constrained — case 1 —	15.34	17.14	22.68
	Index finger constrained — case 2 —	5.29	8.07	9.58
	Difference — (case 2 – case 1) —	–10.05	– 9.07	–13.01
Mediolateral Translation (mm)	Both fingers constrained — case 1 —	0.50	7.06	3.90
	Index finger constrained — case 2 —	5.08	3.72	7.09
	Difference — (case 2 – case 1) —	7.45°	–5.29°	—
Implant Rotation (counterclockwise is positive)	Both fingers constrained — case 1 —	24.63°	6.12°	—
	Index finger constrained — case 2 —	17.18°	11.41°	—
	Difference — (case 2 – case 1) —			

4.3. Inspiration from the Engineering Domain and Animal Models

Our implant was designed with inspiration from the ‘whippletree,’ which is a hierarchically arranged linkage that balances and redistributes force in many applications from horse-drawn carriages to automotive windshield wipers. Its ability to balance force is also used in ‘underactuated’ robot hands [26–31]. Much like in our case, these robot hands sometimes use a single motor to flex four robot fingers adaptively using a whippletree mechanism.

Our work now demonstrates that implantable mechanisms can also use this approach for functional restoration of hand grasp. We arrive at this point after computer simulations, testing on mechanical analogues, such as the Utah-MIT hand, and chicken animal models [6,32,33].

4.4. Implant Design and Fabrication

The implant design (see Figure 1) was driven by three primary goals, (i) improved independent force and movement transmission with a minimal number of components, (ii) secure attachment and integration with the tendons, and (iii) minimize the impact on other anatomical structures.

The implants were 3D printed with Carbon, Inc.’s reinforced polyurethane [12] and used FDA-approved sutures and cyanoacrylate adhesives approved for use in clinical trials. A non-fouling coating minimizes foreign body response and can be sterilized using ethylene oxide [34].

4.5. Considerations When Using Fresh-Frozen Cadaver Specimens

Our study was conducted using fresh-frozen human cadaver specimens obtained from the Anatomical Gift Program at the University of Southern California [35]. This program maintains strict long-term storage, controlled thawing, and preparation protocols for human cadavers. The cadaver specimens were delivered on the morning of the study. Including preparation time by the surgeons and use in the study, the cadavers were outside refrigerated storage for about 4.5 h. Between cadaver preparation and the study, the prepared cadavers were kept refrigerated. As part of preparation, our surgeons resected

unnecessary skin, fat, and muscle tissue from the forearm to slow down decomposition (see Figure 2).

The study was conducted in an air-conditioned Bio-Safety Level 2 (BSL-2) facility maintained at 16 °C. During the study, the cadaver was repeatedly irrigated using medical-grade buffered saline to maintain tissue properties. Previous works involving studies on fresh-frozen human cadavers observed no significant changes to the tendons' biomechanical properties relevant to our work as a result of the freeze-thaw cycle or the 4.5 h experiment duration used here [16,17,36,37].

Additionally, we used computer-controlled precision robotics to quickly perform 200 trials (5 repetitions of 20 paddle orientations at each of 10 input tendon tensions) for each of the four test cases (see Section 2: Testing Protocol) of the rod implant in just 3.5 h. With only three test cases, the U implant was validated in less time. We also had a rehearsal prior to our study to allow time to practice cadaver preparation, instrumentation, and tune our robotic testbed controllers.

4.6. Tissue Abrasion and Foreign Body Response

We conducted initial validations of the implant used in a previous live-chicken study which showed that the implant did not cause tissue abrasion [33]. Hydrogels have also been previously shown to further mitigate foreign body response when used in tandem with our implants in animal models [34].

4.7. Study Limitations

A key limitation of this study is the low number of cadavers used for validating the implants. Each implant is tested only on one hand. Future work will use more cadavers to validate the implant's mechanical efficacy at whole-hand grasp task strength and stability. Additionally, more live animal validation and regulatory work are required before moving to our first in-human trials.

Author Contributions: Conceptualization, S.C.R., K.J., F.J.V.-C. and R.B.; methodology, S.C.R., W.S.Y., K.J., J.C.C., V.R.H., F.J.V.-C. and R.B.; software, S.C.R. and K.J.; validation, S.C.R., W.S.Y., K.J., J.C.C., N.R.L.-M., V.R.H., F.J.V.-C. and R.B.; formal analysis, S.C.R., F.J.V.-C. and R.B.; investigation, S.C.R., W.S.Y., K.J., N.R.L.-M., V.R.H., F.J.V.-C. and R.B.; resources, S.C.R., W.S.Y., F.J.V.-C. and R.B.; data curation, S.C.R., W.S.Y. and F.J.V.-C.; writing—original draft preparation, S.C.R., W.S.Y., K.J., J.C.C., N.R.L.-M., V.R.H., F.J.V.-C. and R.B.; writing—review and editing, S.C.R., W.S.Y., K.J., J.C.C., N.R.L.-M., V.R.H., F.J.V.-C. and R.B.; visualization, S.C.R. and R.B.; supervision, F.J.V.-C. and R.B.; project administration, S.C.R., F.J.V.-C. and R.B.; funding acquisition, S.C.R., F.J.V.-C. and R.B. All authors have read and agreed to the published version of the manuscript.

Funding: This work was partially funded by the US Department of Defense Congressionally Directed Medical Research Program grant number MR150091 awarded to Ravi Balasubramanian and Francisco J. Valero-Cuevas; National Institute of Arthritis and Musculoskeletal and Skin Diseases of the National Institutes of Health grant numbers R01-AR050520 and R01-AR052345, National Institute of Neurological Diseases and Stroke grant number R21-NS113613 and Defense Advanced Research Project Agency L2M grant number W911NF1820264, and National Science Foundation awarded CRCNS US-Japan Award number 2113096 to Francisco J. Valero-Cuevas. Additionally, some work in this manuscript was partly funded by National Science Foundation CAREER award number 1554739 to Ravi Balasubramanian. Finally, this work was also partially funded by the University of Southern California Graduate School's Research Enhancement Fellowship awarded to Suraj Chakravarthi Raja.

Data Availability Statement: The data collected during this study and the code used to process it are available on reasonable requests made to the corresponding author.

Acknowledgments: The authors thank Ali Marjaninejad and Brian A. Cohn for assisting us with the setup of the cadaver studies, Lena Wenske for assisting us with the preparation of the fresh-frozen human cadaver specimens, Anthony Le for helping set up motion-capture and robotic dry-run tests, Sabrina Teo for illustrating our setup Figures 3 and 4, and Rishabh Nagendra and Andrew Erwin for volunteering his time to proofread the manuscript. The authors express their gratitude to the Hand Biomechanics Lab for their donation of the Agee-WristJacks®.

Conflicts of Interest: The research conducted in this work relies on patented designs for the passive mechanisms implanted between the FDP tendons and the ECRL muscle (U.S. Patents 9,925,035 and 10,595,984) granted to Ravi Balasubramanian and Francisco J. Valero-Cuevas along with Taymaz Homayouni. Francisco J. Valero-Cuevas and Ravi Balasubramanian hold equity in OrthoMechanica, Inc. that seeks to commercialize the developed implants. Hand Biomechanics Lab contributed some of the equipment—Agee-WristJacks® and bone pins—used in this study.

Abbreviations

The following abbreviations are used in this manuscript, sorted alphabetically:

DC	Direct Current
ECRL	Extensor Carpi Radialis Longus
EDC	Extensor Digitorum Communis
EIP	Extensor Indicis Proprius
FDA	Food and Drug Administration
FDP	Flexor Digitorum Profundus
FDS	Flexor Digitorum Superficialis
FPL	Flexor Pollicis Longus
MAE	Mean Absolute Error
NI	National Instruments
RPU	Rigid Polyurethane

References

1. Seiler, J.G.; Desai, M.J.; Payne, H.S. Tendon Transfers for Radial, Median, and Ulnar Nerve Palsy. *J. Am. Acad. Orthop. Surg.* **2013**, *21*, 675–684. [[CrossRef](#)] [[PubMed](#)]
2. Sammer, D.M.; Chung, K.C. Tendon Transfers: Part II. Transfers for Ulnar Nerve Palsy and Median Nerve Palsy. *Plastic Reconstr. Surg.* **2009**, *124*, 212e–221e. [[CrossRef](#)]
3. Cooney, W.P. Tendon transfer for median nerve palsy. *Hand Clin.* **1988**, *4*, 155–165. <http://europemc.org/abstract/MED/3294241>. [[CrossRef](#)] [[PubMed](#)]
4. Riordan, D.C. Tendon Transfers for Median, Ulnar or Radial Nerve Palsy. *Hand* **1969**, *1*, 42–46. [[CrossRef](#)]
5. Burkhalter, W.E. Early tendon transfer in upper extremity peripheral nerve injury. *Clin. Orthop. Relat. Res.* **1974**, *104*, 68–79. [[CrossRef](#)]
6. Montgomery, J.; Balasubramanian, R.; Mardula, K.L.; Allan, C.H. New Tendon-Transfer Surgery for Ulnar-Median Nerve Palsy Using Embedded Adaptive Engineering Mechanisms. In Proceedings of the 11th International Symposium, Computer Methods in Biomechanics and Biomedical Engineering, Salt Lake City, UT, USA, 3–6 April 2013; pp. 11–12.
7. Gray, K.; Meals, R.A. Beasley's surgery of the hand: Robert W. Beasley. New York; Thieme Medical Publishers, 2003, 531 pages, \$199.00. *J. Hand Surg.* **2004**, *29*, 336. [[CrossRef](#)]
8. Wangdell, J.; Bunketorp-Käll, L.; Koch-Borner, S.; Fridén, J. Early Active Rehabilitation After Grip Reconstructive Surgery in Tetraplegia. *Arch. Phys. Med. Rehabil.* **2016**, *97*, S117–S125. [[CrossRef](#)]
9. Balasubramanian, R.; Homayouni, T.; Valero-Cuevas, F. Implanted Passive Engineering Mechanisms and Methods for their Use and Manufacture. U.S. Patent 9,925,035, 27 May 2018.
10. Balasubramanian, R.; Homayouni, T.; Valero-Cuevas, F. Implanted Passive Engineering Mechanisms and Methods for their Use and Manufacture. U.S. Patent 10,595,984, 24 May 2020.
11. Mardula, K.L.; Balasubramanian, R.; Allan, C.H. Implanted passive engineering mechanism improves hand function after tendon transfer surgery: A cadaver-based study. *Hand* **2015**, *10*, 116–122. [[CrossRef](#)]
12. Carbon3D. Carbon3D Rigid Polyurethane (RPU 70). 2022. Available online: <https://carbon3d.com/materials/rpu-70/> (accessed on 14 December 2022).
13. Hand Biomechanics Lab. Agee-WristJack Surgeon's Manual. 2002. Available online: <https://handbiolab.com/wp-content/uploads/2017/09/WJSM-306000R.pdf> (accessed on 14 December 2022).
14. Hand Biomechanics Lab. Agee-WristJack. 2022. Available online: <https://handbiolab.com/products/wristjack/> (accessed on 14 December 2022).
15. McMaster-Carr. High-Strength High-Temperature Para-Aramid Thread: 0.038" Diameter—Mcmaster Carr Part #8800K43. 2022. Available online: <https://www.mcmaster.com/8800K43/> (accessed on 14 December 2022).
16. Jalaleddini, K.; Minos Niu, C.; Chakravarthi Raja, S.; Joon Sohn, W.; Loeb, G.E.; Sanger, T.D.; Valero-Cuevas, F.J. Neuromorphic meets neuromechanics, part II: The role of fusimotor drive. *J. Neural Eng.* **2017**, *14*, 025002. [[CrossRef](#)]
17. Niu, C.M.; Jalaleddini, K.; Sohn, W.J.; Rocamora, J.; Sanger, T.D.; Valero-Cuevas, F.J. Neuromorphic meets Neuromechanics PART I: The Methodology and Implementation. *J. Neural Eng.* **2017**, *14*, 025001. [[CrossRef](#)]

18. Adept Technology Inc. *AdeptSix 300 Instruction Handbook*; Data Sheet 00660–00100; Regional Headquarter Omron Adept: San Eamon, CA, USA, 2005.
19. Johanson, M.E.; Smaby, N.; Murray, W.M.; Hentz, V.R. The effect of task demand on pinch force magnitude in subjects with spinal cord injury. *J. Neurol. Phys. Ther.* **2007**, *31*, 197–198.
20. Johanson, M.E.; Murray, W.M. The unoperated hand: The role of passive forces in hand function after tetraplegia. *Hand Clin.* **2002**, *18*, 391–398. [[CrossRef](#)]
21. Mehta, V.; Phillips, C.S. Flexor Tendon Pulley Reconstruction. *Hand Clin.* **2005**, *21*, 245–251. [[CrossRef](#)]
22. Uchiyama, S.; Coert, J.H.; Berglund, L.; Amadio, P.C.; An, K.N. Method for the measurement of friction between tendon and pulley. *J. Orthop. Res.* **1995**, *13*, 83–89. [[CrossRef](#)] [[PubMed](#)]
23. Petersen, W.; Stein, V.; Bobka, T. Structure of the human tibialis anterior tendon. *J. Anat.* **2000**, *197*, 617–625. [[CrossRef](#)] [[PubMed](#)]
24. Lee, D.H.; Oakes, J.E.; Ferlic, R.J. Tendon transfers for thumb opposition: A biomechanical study of pulley location and two insertion sites. *J. Hand Surg.* **2003**, *28*, 1002–1008. [[CrossRef](#)]
25. Skie, M.C.; Parent, T.; Mudge, K.; Dai, Q. Kinematic Analysis of Six Different Insertion Sites for FDS Opponensplasty. *HAND* **2010**, *5*, 261–266. [[CrossRef](#)]
26. Hsu, J.; Yoshida, E.; Harada, K.; Kheddar, A. Self-locking underactuated mechanism for robotic gripper. In Proceedings of the 2017 IEEE International Conference on Advanced Intelligent Mechatronics (AIM), IEEE, Munich, Germany, 3–7 July 2017; pp. 620–627. [[CrossRef](#)]
27. Balasubramanian, R.; Santos, V.J. (Eds.) *The Human Hand as an Inspiration for Robot Hand Development*; Springer Tracts in Advanced Robotics; Springer International Publishing: Cham, Swizterland, 2014; Volume 95. [[CrossRef](#)]
28. You, W.S.; Lee, Y.H.; Kang, G.; Oh, H.S.; Seo, J.K.; Choi, H.R. Kinematic design optimization for anthropomorphic robot hand based on interactivity of fingers. *Intell. Serv. Robot.* **2019**, *12*, 197–208. [[CrossRef](#)]
29. Ma, R.R.; Odhner, L.U.; Dollar, A.M. A modular, open-source 3D printed underactuated hand. In Proceedings of the 2013 IEEE International Conference on Robotics and Automation, IEEE, Karlsruhe, Germany, 6–10 May 2013; pp. 2737–2743. [[CrossRef](#)]
30. Kragten, G.A.; Herder, J.L. The ability of underactuated hands to grasp and hold objects. *Mech. Mach. Theory* **2010**, *45*, 408–425. [[CrossRef](#)]
31. Kontoudis, G.P.; Liarokapis, M.V.; Zissimatos, A.G.; Mavrogiannis, C.I.; Kyriakopoulos, K.J. Open-source, anthropomorphic, underactuated robot hands with a selectively lockable differential mechanism: Towards affordable prostheses. In Proceedings of the 2015 IEEE/RSJ International Conference on Intelligent Robots and Systems (IROS), IEEE, Hamburg, Germany, 28 September 2015–2 October 2015; pp. 5857–5862. [[CrossRef](#)]
32. Pihl, C.M.; Stender, C.J.; Balasubramanian, R.; Edinger, K.M.; Sangeorzan, B.J.; Ledoux, W.R. Passive engineering mechanism enhancement of a flexor digitorum longus tendon transfer procedure. *J. Orthop. Res.* **2018**, *36*, 3033–3042. [[CrossRef](#)]
33. Browning, G.R.; Le, A.H.; Warnock, J.J.; Balasubramanian, R. An Investigation of a Novel Tendon Transfer Surgery for High Median–Ulnar Nerve Palsy in a Chicken Model. *J. Investig. Surg.* **2019**, *32*, 39–47. [[CrossRef](#)]
34. Zhang, L.; Cao, Z.; Bai, T.; Carr, L.; Ella-Menyé, J.R.; Irvin, C.; Ratner, B.D.; Jiang, S. Zwitterionic hydrogels implanted in mice resist the foreign-body reaction. *Nat. Biotechnol.* **2013**, *31*, 553–556. [[CrossRef](#)] [[PubMed](#)]
35. University of Southern California. The Anatomical Gift Program at USC. 2023. Available online: <https://agp.usc.edu/> (accessed on 28 April 2023).
36. Clavert, P.; Kempf, J.F.; Bonnomet, F.; Boutemy, P.; Marcellin, L.; Kahn, J.L. Effects of freezing/thawing on the biomechanical properties of human tendons. *Surg. Radiol. Anat.* **2001**, *23*, 259–262. [[CrossRef](#)] [[PubMed](#)]
37. Van Ee, C.A.; Chasse, A.L.; Myers, B.S. The effect of postmortem time and freezer storage on the mechanical properties of skeletal muscle. *SAE Trans.* **1998**, *107*, 2811–2820. <http://www.jstor.org/stable/44741238>.

Disclaimer/Publisher’s Note: The statements, opinions and data contained in all publications are solely those of the individual author(s) and contributor(s) and not of MDPI and/or the editor(s). MDPI and/or the editor(s) disclaim responsibility for any injury to people or property resulting from any ideas, methods, instructions or products referred to in the content.